MOLECULAR ECOLOGY

Molecular Ecology (2017) **26**, 3241–3255 doi: 10.1111/mec.14114

Perpendicular axes of differentiation generated by mitochondrial introgression

HERNÁN E. MORALES,*† PAUL SUNNUCKS,* LEO JOSEPH‡ and ALEXANDRA PAVLOVA*

*School of Biological Sciences Monash University, Clayton Campus, Melbourne, Vic. 3800, Australia, †Centre for Marine Evolutionary Biology, Department of Marine Sciences, University of Gothenburg, Box 461, SE 405 30, Göteborg, Sweden, ‡Australian National Wildlife Collection, CSIRO National Research Collections Australia, GPO Box 1700, Canberra, ACT 2601, Australia

Abstract

Differential introgression of mitochondrial vs. nuclear DNA generates discordant patterns of geographic variation and can promote population divergence and speciation. We examined a potential case of mitochondrial introgression leading to two perpendicular axes of differentiation. The Eastern Yellow Robin *Eopsaltria australis*, a widespread Australian bird, shows a deep mitochondrial split that is perpendicular to north–south nuclear DNA and plumage colour differentiation. We propose a scenario to explain this pattern: (i) first, both nuclear and mitochondrial genomes differentiated in concert during north–south population divergence; (ii) later, their histories disconnected after two mitochondrial introgression events resulting in a deep mitochondrial split perpendicular to the nuclear DNA structure. We explored this scenario by coalescent modelling of ten mitochondrial genes and 400 nuclear DNA loci. Initial mitochondrial and nuclear genome divergences were estimated to have occurred in the early Pleistocene, consistent with the proposed scenario. Subsequent climatic transitions may have driven later mitochondrial introgression. We consider neutral introgression unlikely and instead propose that the evidence is more consistent with adaptive mitochondrial introgression and selection against incompatible mitochondrial-nuclear combinations. This likely generated an axis of coastal-inland mitochondrial differentiation in the face of nuclear gene flow, perpendicular to the initial north–south axis of differentiation (reflected in genomewide nuclear DNA and colour variation).

Keywords: adaptive introgression, coalescence, mitochondria, mitonuclear, selective sweep

Received 16 October 2016; revision received 14 March 2017; accepted 15 March 2017

Introduction

When divergent populations undergo hybridization, genes from one population can be incorporated into the other (i.e. there is introgression) to a variable extent within and between genomes (Harrison & Larson 2014, 2016). Alleles that are not involved in local adaptation and that have not accumulated incompatibilities with other loci are expected to move freely between populations (Mallet 2005). On the other hand, if genes from one population improve fitness in the other population, adaptive introgression can occur (Hedrick 2013). The proportion of the genome that is resistant or prone to introgression can vary as a result of local adaptation in heterogeneous environments and demographic history (Harrison & Larson 2014). Therefore, differential rates of introgression offer a valuable insight into adaptive divergence and speciation (Payseur 2010; Rheindt & Edwards 2011).

Differential rates of introgression of mitochondrial DNA (mtDNA) vs. nuclear DNA (nDNA) genes are a main cause of mitochondrial-nuclear (mitonuclear) discordances (Toews & Brelsford 2012). However, it is challenging to predict the conditions under which higher rates of mitochondrial or nuclear introgression can be expected. This is because genetic patterns in both genomes can differently reflect the effects of genetic drift and selection, and the two genomes have different modes of inheritance and recombination

Correspondence: Hernán E. Morales, Fax: +46 31 786 13 33; E-mail: hern.moral@gmail.com

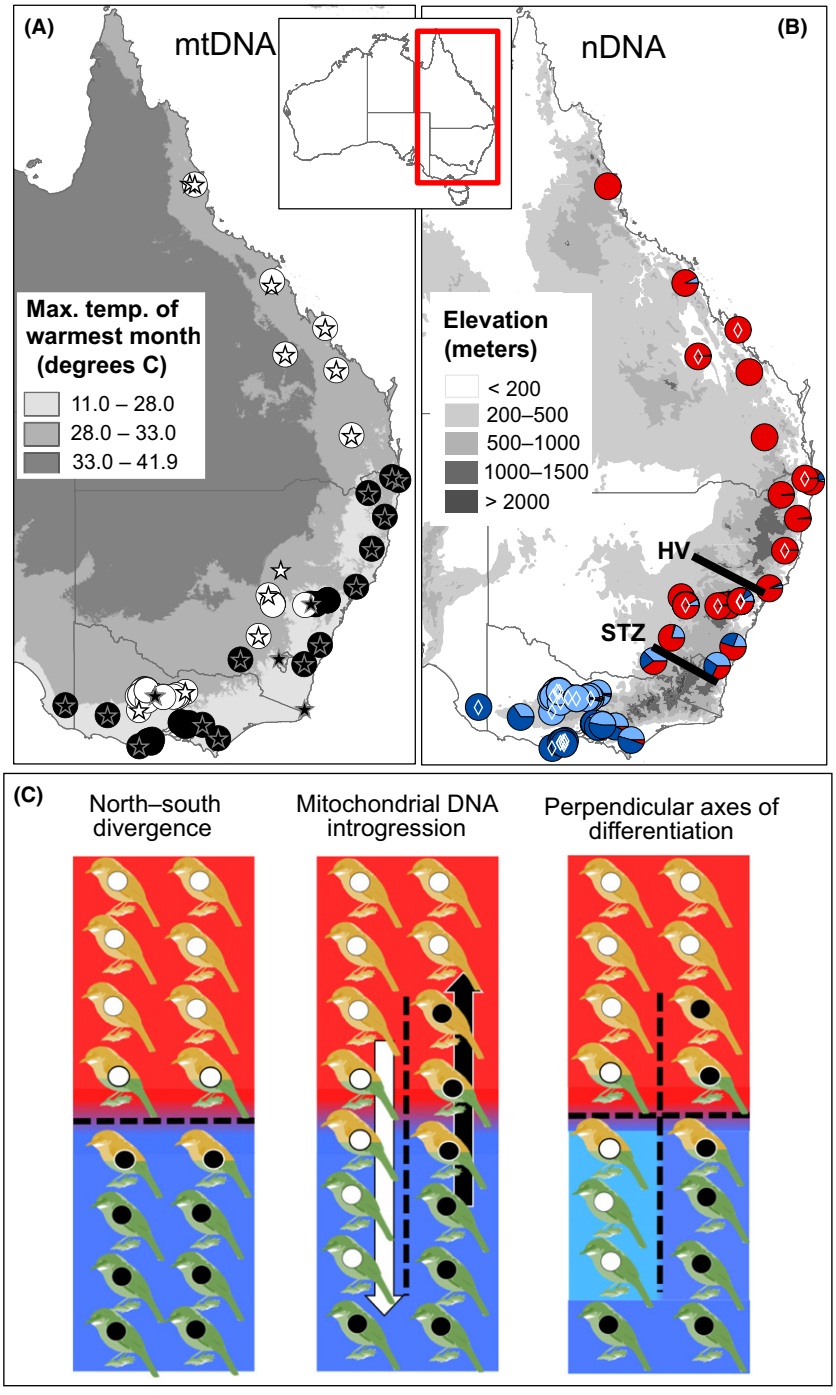

(Harrison 1990; Funk & Omland 2003). In addition, demographic and ecological factors including population density, sex-ratio, mating behaviour, sex-bias in dispersal and episodes of spatial invasion impact expectations for nuclear and mitochondrial gene flow (Currat *et al.* 2008; Petit & Excoffier 2009). These considerations have generated the counter-intuitive proposal that hybridizing populations will typically experience less gene flow between them in markers that experience more gene flow within populations (Petit & Excoffier 2009). A test of this in 37 case studies revealed that 16/16 hybridization scenarios with female-biased dispersal had less mtDNA than nDNA gene flow between them, while the reverse was true for most male-biased dispersers (Petit & Excoffier 2009). Moreover, low passage through hybrid zones of maternally transmitted mtDNA is predicted for species with heterogametic females, such as birds, under Haldane's Rule (i.e.

Fig. 1 Distribution of Eastern Yellow Robin samples used in this study showing their contribution to mitochondrial (A) and nuclear (B) genetic structures and a schematic representation of EYR evolutionary history (C). (A) Distribution of mitochondrial lineages mito-A (white) and mito-B (black) plotted over the maximum temperature of the warmest month. Circles represent samples sequenced for the mitochondrial ND2 gene, stars-samples for which data from 10 mitochondrial genes were used. (B) Distribution of samples for which nuclear loci were sequenced, mapped over elevation map featuring the Great Dividing Range (dark shading); pies show individual membership in three genetic populations according to $K = 3$ STRUCTURE analysis (see Fig. 2A): northern population (red), southern coastal population (dark blue) and southern inland population (light blue). Samples used for IMa2 analysis are indicated with white diamonds. Black lines represent potential vicariant/environmental barriers, HV—Hunter Valley and STZ—Southern Transition Zone. (C) Evolutionary history of the Eastern Yellow Robin, the colours of the boxes represent their nuclear genomic background (colour of the background; north = red and south = blue), their plumage coloration (colour of the birds; northern yellow, southern green and intermediates of mixed colour), and their mitochondrial membership (colour of the circles; mito-A = white and mito-B = black). First panel shows the first axis of differentiation: mtDNA, nDNA and colour differentiation between northern and southern birds with a zone of intergradation. The second panel shows the second axis of differentiation: two independent events of mitochondrial introgression occurred without nDNA introgression, resulting in mtDNA genetic structure in the inland-coastal direction. The third panel shows the current perpendicular pattern of differentiation: inland-coast mitochondrial divergence in the face of nuclear gene flow, major north–south nDNA structure and plumage coloration divergence and a minor inland-coast nuclear DNA divergence in the southern range (shades of blue).

disproportional hybrid sterility and/or inviability of the heterogametic sex; Haldane 1922). These predictions are commonly supported by studies of avian hybrid zones (Rheindt & Edwards 2011). On the other hand, higher mtDNA than nDNA introgression can occur if a population of low effective size accumulates slightly deleterious mutations by drift (i.e. builds up mitochondrial mutation load) to the point where mitochondrial replacement (by introgression) from neighbouring populations is needed (Sloan *et al.* 2016). Moreover, high mtDNA introgression can stem from female-biased dispersal (Petit *et al.* 2004) and asymmetrical mating success of females from hybridizing populations (Roca *et al.* 2005), where females that are more dispersive and/or reproductively successful will transmit maternally inherited mtDNA more often. Alternatively to all the nonadaptive explanations above, adaptive mitochondrial introgression into a beneficiary population could be common given the importance of mtDNA for organismal metabolism and fitness (Currat *et al.* 2008; Toews & Brelsford 2012; Hedrick 2013).

The Eastern Yellow Robin (*Eopsaltria australis*, hereafter EYR) shows a striking pattern of geographic mitonuclear discordance, representing an excellent system to study differential mtDNA and nDNA introgression (Pavlova *et al.* 2013). The two major mitochondrial lineages of EYR (mitolineages; mito-A and mito-B) are 6.8% divergent and structured across inland and coastal sides of the Great Dividing Range in southeastern Australia (Pavlova *et al.* 2013; Fig. 1A). In contrast, the major axis of nDNA structure runs north–south through the species range (Fig. 1B). Thus, nDNA and mtDNA structures are geographically perpendicular (Pavlova *et al.* 2013; Fig. 1A, B). Additionally, minor inland-coastal nDNA structure exists in the south corresponding with mitolineage distributions (Morales *et al.* 2016a; Fig. 1B). The major north–south axis of nDNA differentiation is mirrored by rump plumage colour variation, supporting two currently recognized subspecies: the rump is bright yellow in northern *E. a. chrysorrhoa*, and olive-green in southern *E. a. australis* (Ford 1979; Schodde & Mason 1999). Colour variation at the continental-scale is strongly influenced by population history, but on a regional scale appears to be structured according to local environmental variation (Morales *et al.* 2016a).

Previous studies have considered drivers of observed patterns of genetic and phenotypic variation in EYR. Using microsatellites, nuclear intron sequences and one mitochondrial gene, Pavlova *et al.* (2013) rejected three common explanations of mitonuclear discordance based on selective neutrality (Toews & Brelsford 2012): (i) inland-coast vicariance was not supported by models of past and present species distributions, (ii) incomplete lineage sorting was contradicted by the >1500 km extent of the mitolineage contact zone and inferred nuclear gene flow between mitolineages, and (iii) male-biased dispersal is counter to known female-biased dispersal in EYR (Debus & Ford 2012; Harrisson *et al.* 2012). They found that maximum temperature of the hottest month explains mtDNA variance over and above that explained by geographic position and distance, which suggests environmental temperature as a possible selective driver of mitolineage distribution (Fig. 1A). Pavlova *et al.* (2013) concluded that the major nDNA north–south structure in EYR was consistent with isolation by distance, and that inland-coastal mtDNA divergence occurred in situ. Subsequently, Morales *et al.* (2015) found evidence supporting selection on mitochondrial genomes and confirmed extremely low mitogenomewide intralineage diversity consistent with selective sweeps. Morales *et al.* (2016a) expanded the analysis of nDNA by analysing genome-wide neutral single nucleotide polymorphisms (SNPs) and argued for the presence of two genetic populations,

northern and southern, with a zone of intergradation, modifying the previously inferred isolation by distance. They also showed that plumage colour differentiation follows a similar geographic trend, albeit with a broader zone of intergradation. Reconstructions of the evolutionary histories of each genome are needed to better understand mitonuclear discordance in EYR, an emerging model of mitonuclear interactions and lineage divergence.

Here, we propose a novel scenario to explain perpendicular mitonuclear differentiation in EYR (Fig. 1C). Initial north–south divergence could have generated concordant mtDNA and nDNA divergence, currently reflected in the major nDNA structure and colour variation (first axis of differentiation) but not in mtDNA structure. Subsequently, independent events of mitochondrial introgression might have occurred with little associated nDNA introgression, one south-to-north coastwards of the Great Dividing Range, and the other north-to-south inland of the Great Dividing Range. Mitochondrial introgression would thus have resulted in the current inland-coastal mitochondrial split and inland-coast mitonuclear divergence-with-gene-flow in the southern population (a second axis of differentiation). We used a coalescent multilocus approach to explore this scenario by analysing 10 mitochondrial genes, and 400 sequenced nuclear loci. We estimated nuclear divergence times, geneflow rates and effective population sizes and tested whether the onset of mitochondrial divergence coincided with north–south population divergence. We discuss our findings in the context of adaptive mitochondrial evolution, introgression and mitonuclear co-evolution (Dowling *et al.* 2008; Gershoni *et al.* 2009; Burton *et al.* 2013; Hill 2015, 2016).

Methods

Samples, molecular methods and data sets

We analysed (i) mitochondrial ND2 sequences, (ii) 2728 SNPs and (iii) phased alleles for 400 nuclear sequences for 69 individuals and (4) 10 mitochondrial genes for 32 individuals (Fig. 1A, B). Genomic DNA from 42 newly collected blood samples was extracted with DNAeasy Kit (Qiagen, Germany) following the manufacturer's protocol. For these samples, a partial region (~1000 bp) of mitochondrial ND2 gene was amplified following Pavlova *et al.* (2013) and sequenced commercially (Macrogen, Korea). The newly produced ND2 data set was supplemented with previously published ND2 sequences for 27 individuals (GenBank accession in Table S1, Supporting information; Pavlova *et al.* 2013). Based on ND2, all 69 individuals were assigned to one of the two mitolineages (35 mito-A and 34 mito-B; Table S1, Supporting information; black and white circles on Fig. 1A).

For the same 69 individuals, 1000 sequenced anonymous nuclear loci were obtained by hybrid capture enrichment probes (size = 240 bp; Lemmon *et al.* 2012). Probe design was optimized using a draft of the EYR genome (Morales, Wang, Pavlova and Sunnucks, unpublished data; sample code: EYR056, Lat/Long: 143.41/−36.79). Briefly, DNA for genome sequencing was prepared into one paired-end (500 bp insert size, 100-bp read length) and one mate-pair (2 kb insert size, 50-bp read length) library. Libraries were prepared and sequenced with standard Illumina HiSeqTM 200 protocols at the Beijing Genome Institute. The paired-end library produced 34 913 million bases and the mate-pair library 10 976 million bases. De novo assembly was performed with SOAPDENOVO version 1.05 with a K-mer size of 35 and default settings (Li *et al.* 2010). Capture probes included sequenced regions with 40% and 55% GC content, low-copy number and with at least 96% average identity across mapped reads. Probes were tiled uniformly at 2× density (three probes per locus) to form the probe set. Indexed libraries were prepared from genomic DNA and enriched using an Agilent Sure Select enrichment kit. Libraries were sequenced on an Illumina 2500 lane with paired-end 150-bp reads and 8 bp indexing read.

The SNP data set consisted of 2728 SNPs, previously used by Morales *et al.* (2016a). They were obtained as follows: reads were mapped against the capture probe references with BWA version 0.7.12 (Li & Durbin 2009), PCR duplicates were removed, and InDel re-alignment was performed with PICCARD version 1.138 (http://broadinstitute.github.io/picard/). SNP-calling was performed with the UnifiedGenotype in GATK version 3.4 (DePristo *et al.* 2011). SNPs were filtered according to overall quality ≥100, mapping quality ≥20, depth ≥5, Phred score ≥20, heterozygosity ≤0.8, minor allele frequency ≥0.05 and genotype frequency ≥90%.

The phased allele data set consisted of 400 nuclear sequences. Postprocessing of targeted captured loci including raw sequencing reads manipulation read assembly, orthology calculations and sequence alignment was performed following Prum *et al.* (2015) (accompanying scripts can be found at doi: 10.5281/zenodo.28343). Allele phasing for each locus was determined statistically from the assembled reads by drawing a posterior distribution for each individual separately, following Pyron *et al.* (2016); for methodological details and scripts see doi: 10.5061/dryad.51v22. In short, the method generates alleles with no ambiguities for positions that can be phased with a ≥95% posterior probability confidence, leaving ambiguities for the remainder of the polymorphic sites. We

randomly selected 400 loci from the resulting phased alignments for coalescent analyses (the maximum number of loci accepted by IMa2).

To appropriately assign inheritance scalars for the sequenced loci in the IMa2 analysis (below), we mapped the alignment consensus sequences to the Zebra Finch *Taeniopygia guttata* genome TAEGUT 3.2.4 (Warren *et al.* 2010) using BLASTN version 2.3.0 (Camacho *et al.* 2009) with a *E*-value threshold of 1×10^{-4} (BLAST output doi: 10.6084/m9.figshare.3581004). Because historical inferences assume neutral evolution, we identified all nuclear loci that may have evolved under directional selection (outlier loci) and removed them from the SNP and phased sequences data sets. Outlier loci were identified with LOSITAN (Antao *et al.* 2008) with samples divided into 10 populations based on their geographic location (Fig. 2B). All the data used in this project (capture probes for the EYR hybrid capture enrichment, raw reads and phased sequence alignments) have been deposited in figshare (doi: 10.6084/m9.figshare.3581004) and SRA (Accession no. SRP079228) online repositories.

Sequences of 10 protein-coding mitochondrial genes (ND1, ND2, ND3, ND5, ND6, COX1, COX2, COX3, ATP6 and ATP8) were extracted from 32 published mitogenome sequences (14 mito-A and 18 mito-B, represented by stars on Fig. 1A; GenBank accessions in Table S2, Supporting information; Morales *et al.* 2015). These genes were chosen because they did not show signatures of positive selection between mitolineages (Morales *et al.* 2015).

Nuclear DNA genetic structure

We used the SNP data set and admixture model with correlated allele frequencies implemented in STRUCTURE 2.3.4 (Pritchard *et al.* 2000) to confirm the presence of major and minor nDNA structure and assign each individual to one of three populations (northern, south-inland and south-coast: red, light blue and dark blue on Fig. 1C, respectively) for IMa2 analysis (below). To meet STRUCTURE assumptions that loci are in linkage and Hardy–Weinberg equilibrium (HWE), we (i) subsampled one SNP per locus (i.e. per capture probe) and (ii) filtered out loci not in HWE with the HWE.test.genind function in the R package ADEGENET 2.0.0 (Jombart & Ahmed 2011; R Development Core Team 2014). The

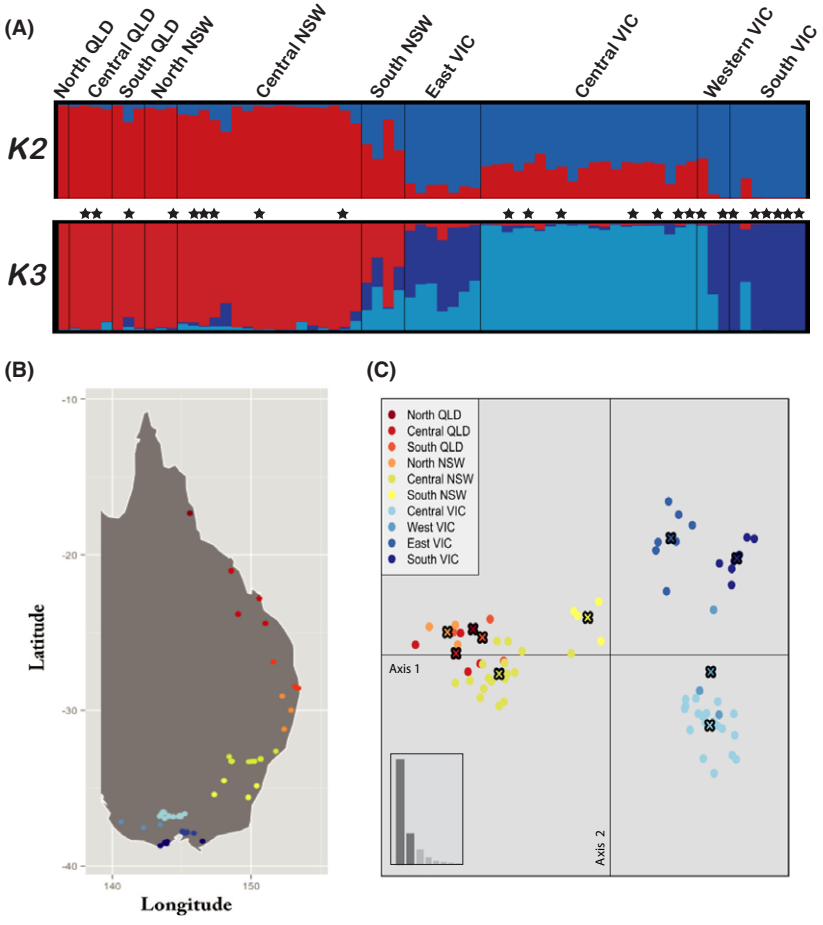

Fig. 2 Summary of population genetic structure in the Eastern Yellow Robin. (A) The results of STRUCTURE (Pritchard *et al.* 2000) models when $K = 2$ and $K = 3$. Results were summarized with STRUCTURE HARVESTER WEB version 0.6.94 (Earl 2012) and CLUMPP version 1.1.2 (Jakobsson & Rosenberg 2007). Samples used for IMa2 analysis are indicated with black stars. (B) Map of samples used for the nuclear DNA data arranged into arbitrary populations according to geographic position. (C) Discriminant analysis of principal components (DAPC; Jombart *et al.* 2010) for populations from panel B, axis 1 (PC1) captured 48% of genetic variation and axis 2 (PC2) captured 12% of genetic variation.

initial significance level ($\alpha < 0.05$) of the HWE test was corrected for multiple tests using the B–Y method to account for false discovery rate (FRD < 1%) following Narum (2006). To reduce Wahlund effect, which could cause loci to be falsely concluded to deviate from HWE through non-Mendelian inheritance, samples were divided into 10 populations based on their geographic location (Fig. 2B from the main text). The filtering process resulted in a reduced data set of 706 SNPs. STRUCTURE analyses were performed assuming 1–5 genetic populations (K) with 25 independent Markov chains of 200 000 iterations of burn-in and 80 000 recorded iterations for each K. Convergence of the parameters alpha and log likelihood across chains was determined for every K value with custom R scripts (Gonçalves da Silva, 2016; https://zenodo.org/record/48790#.V3KiXZN96Rs). Results were summarized and the optimal number of populations estimated with the Evanno test (Evanno *et al.* 2005) in STRUCTURE HARVESTER WEB version 0.6.94 (Earl 2012). Average Q-values across replicates were obtained with CLUMPP version 1.1.2 (Jakobsson & Rosenberg 2007). Individuals with a posterior probability (Q-values) of ≥0.8 of belonging to a particular population were assigned to that genetic population.

We used discriminant analysis of principal components (DAPC: Jombart *et al.* 2010) implemented in ADEGENET to estimate the amount of genetic variation explained by the major and minor axes of nDNA structure. The DAPC analysis was conducted with 10 populations delimited based on their geographic location (Fig. 2B). To estimate the number of loci contributing to the observed nDNA genetic structure, we performed a pairwise Nei's G_{ST} (Nei 1973) test between samples unambiguously assigned to populations by STRUCTURE (i.e. assignment probability of $Q > 0.8$ from $K = 3$ STRUCTURE analysis, see Results) using the same unlinked 706 SNPs. We created genind objects for each pairwise comparison with the R package ADEGENET (Jombart & Ahmed 2011) and 1000 bootstrap samples, with each subpopulation resampled according to its size, with the function chao_bootstrap of the mmod R package (Winter 2012). Then, for each set of permuted data set, we obtained the observed per-locus Nei's G_{ST} value and its normalized 95% confidence intervals (CI) (i.e. centred on the observed value and corrected with standard deviation across replicates) with the function summarise_bootstrap in mmod. Loci were considered significantly differentiated if the lower bound of the CI was greater than zero.

Isolation-with-migration models

To estimate times of population divergence, gene flow and effective population sizes, we fitted a three-population model of isolation with migration (Hey & Nielsen 2004) implemented in IMa2 (Hey 2010) to the multilocus data set comprising sequences of 400 randomly selected anonymous nuclear loci. For each locus, the longest stretch of each sequence without ambiguities was used. Recombination points were detected for each locus with the program IMGC (Woerner *et al.* 2007) and the longest nonrecombining block was retained. Resulting alignments had lengths from 124 to 529 bp (mean = 264 bp). IMa2 estimates model parameters scaled by mutation rate (μ), population divergence time in generations ($t = t\mu$), migration rate ($m = m/\mu$) and effective population sizes ($\theta = 4Ne\mu$). Inheritance scalars were set to 1.0 for autosomes and 0.75 for Z-linked loci.

To estimate historical gene flow between three largely panmictic populations, we subsampled 'pure' individuals from each population (based on $Q > 0.8$ from $K = 3$ STRUCTURE analysis), avoiding admixed individuals from putative contemporary hybrid zones. Individuals with a posterior probability (Q-values) of population membership <0.8 were not used in the analysis because they could not be assigned to any population unambiguously, and arbitrary assignment would inevitably add stochasticity to the divergence estimates. As a result, we have likely underestimated gene flow among contemporary populations. We accepted this compromise because precise estimates of divergence were essential whereas slightly imprecise estimates of gene flow were acceptable given our aims. Moreover, to avoid excessive IMa2 computation time inherent to analyses with very large numbers of loci, we further subsetted the data set by randomly selecting individuals from the 'pure' populations (northern: $N = 9$ individuals, 18 alleles, southern inland: $N = 7$ individuals, 14 alleles, and southern coastal: $N = 8$ individuals, 16 alleles, Table S1, Supporting information and Fig. 1B). Sixteen parameters were estimated: two of t, eight of m and six of θ (θs were estimated at three time intervals: $t1$, $t0$ and present; model option j5; see legend of Fig. 3A). Multiple preliminary analyses were run to optimize prior parameter boundaries. Eight independent replicates were run for the final analysis, each involved $>11 \times 10^6$ steps after a burn-in period of $>4.8 \times 10^5$ steps, employing 150 MCMC chains with geometric heating (parameters $a = 0.999$ and $b = 0.3$). Parameter estimates were converted to demographic units using a generation time of 3.5 years (Pavlova *et al.* 2013) and a mutation rate of 1.2×10^{-9} (lower bound = 0.7×10^{-9}; upper bound = 2.5×10^{-9}) nucleotides per base per year, which have been used to estimate demographic parameters in passerines (Ellegren 2007; Lee & Edwards 2008). The mutation rates we used incorporate a wide range of values that have seen previously to capture most rates of slow-evolving introns (Ellegren 2007) and of faster-evolving anonymous loci (Lee & Edwards

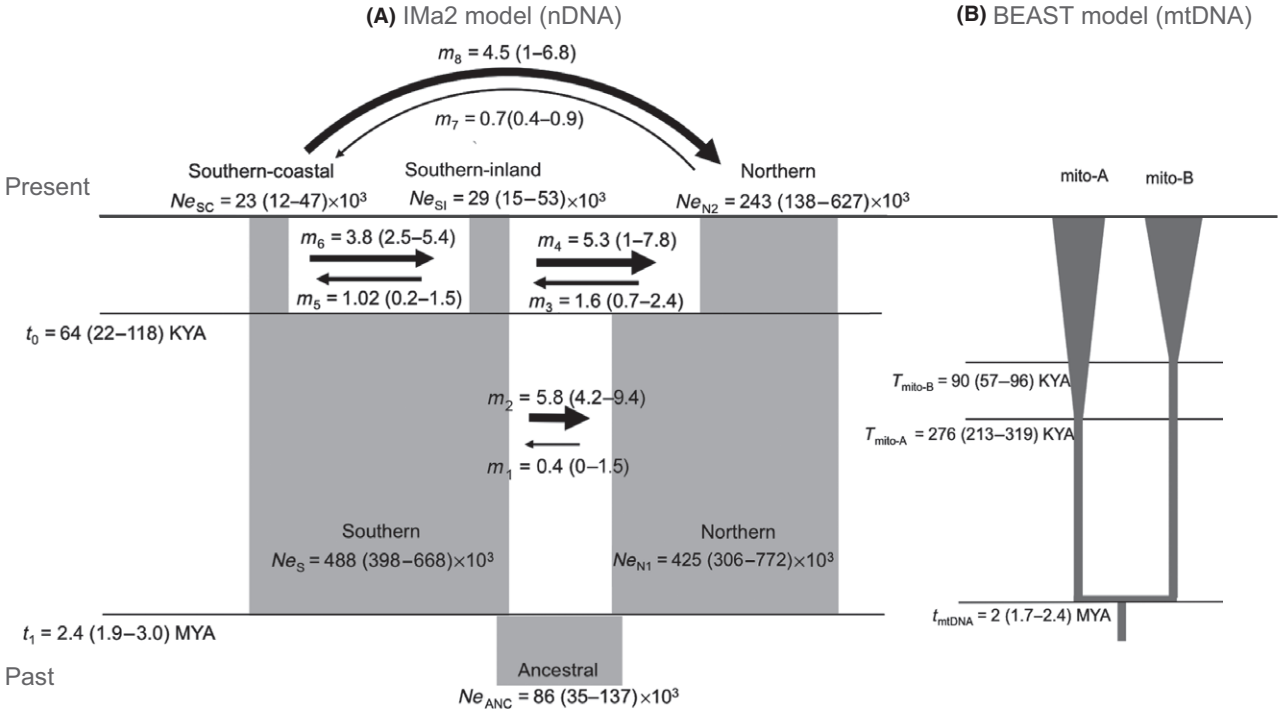

Fig. 3 Estimates [high point (95% HPDs)] of coalescent analyses in IMa2 (400 nDNA loci) and BEAST (10 mtDNA genes). (A) IMa2 model. Divergence times: ($t1$) northern vs. southern ancestral populations; ($t0$) southern coastal vs. southern inland populations. Effective population size (Ne): (Ne_{ANC}) ancestral root population; (Ne_{N1}) ancestral northern population; (Ne_S) ancestral southern population; (Ne_{N2}) northern population; (Ne_{SC}) southern coastal population; (Ne_{SI}) southern inland population. Gene flow: ($m1$) ancestral northern to ancestral southern; ($m2$) ancestral southern to ancestral northern; ($m3$) northern to southern inland; ($m4$) southern inland to northern; ($m5$) southern inland to southern coastal; ($m6$) southern coastal to southern inland; ($m7$) northern to southern coastal; ($m8$) southern coastal to northern. (B) BEAST mitolineage model. Divergence times (t_{mtDNA}) between mitolineages mito-A and mito-B. Time to the most recent common ancestor (TMRCA) for ($T_{mito\text{-}A}$) mitolineage mito-A and ($T_{mito\text{-}B}$) mitolineage mito-B indicate probable times of mitochondrial selective sweeps.

2008). Moreover, this conservative approach allows IMa2 to directly infer per-locus mutation rates from a wide range of prior values.

Mitochondrial lineage divergence

To test for simultaneous divergence of mitolineages (mito-A and mito-B) and nuclear DNA, we built a calibrated phylogeny in BEAST version 1.8.0 (Drummond *et al.* 2012) using sequences of 10 protein-coding mitochondrial genes that are free from signatures of positive selection. Although mitolineage divergence time was estimated previously from ND2 [1.5 (0.98–2.15) million years ago (MYA); Pavlova *et al.* 2013], by using multiple genes we improve the precision of the estimate. The optimal partitioning scheme and substitution models were identified using PartitionFinder (Lanfear *et al.* 2012; Table S3, Supporting information). Linked trees, linked clock models, and unlinked substitution models were used. We performed four replicates with 8×10^7 generations sampled every 2000 steps after 10% of burn-in. The four independent runs were combined and convergence checked in TRACER version 1.6.0 (Rambaut *et al.* 2014). Mitolineage divergence time was calibrated assuming neutral evolution rates for mitochondrial genes of the Hawaiian honeycreeper (Lerner *et al.* 2011). To apply honeycreeper mutation rates to the EYR, we assume that rates among passerines should be similar, that strong purifying selection acting on the EYR mitogenome should also act on the honeycreeper mitogenome, and that we prevent major bias of diversifying selection by avoiding genes with evidence of positive selection (Morales *et al.* 2015).

Results

Nuclear DNA genetic structure

The STRUCTURE models with two and three populations (K = 2: LnP(K) = −38224.17; ΔK = 217.1 and K = 3: LnP(K) = −37503.8; ΔK = 225.9) reached convergence for all chains (Figs S1–S2, Supporting information). These supported two main populations (northerly and southerly) with some individuals displaying intermediate

assignment scores (red and blue in Figs 1B and 2A; Table S1, Supporting information). The higher likelihood model assuming $K = 3$ (Fig. S3, Supporting information) further subdivided the southern population into inland and coastal populations, in which all inland individuals ($Q > 0.8$) belong to mito-A mitolineage, and coastal individuals to mito-B mitolineage (shades of blue in Figs 1B and 2A). $K = 4$ and $K = 5$ analyses did not show any additional geographically meaningful structure (not shown). DAPC showed that 48% of genetic variation is explained by the major north–south structure (PC1 on Fig. 2C), and 12% is explained by the minor southerly inland-coast structure (PC2 on Fig. 2C). The number of polymorphic loci considered for the pairwise G_{ST} test was as follows: north vs. south-coastal = 574; north vs. south-inland = 628; south-inland vs. south-coastal = 605. Mean pairwise G_{ST} estimates were low to medium for all population comparisons; mean G_{ST} (mean 95% CI): north vs. south-coastal = 0.09 (0.02–0.18); north vs. south-inland = 0.07 (−0.03 to 0.19); south-inland vs. south-coastal = 0.04 (−0.02 to 0.11). The two north–south comparisons had more significantly differentiated SNPs than the comparisons between the southern populations: north vs. south-coastal = 284 SNPs (49%); north vs. south-inland = 188 SNPs (30%); south-inland vs. south-coastal = 141 SNPs (23%) (Fig. S4, Supporting information).

Population divergence: isolation-with-migration model

Convergence of IMa2 parameter estimates was confirmed by lack of trends on parameter plots, similarity of estimates across replicate and appropriate mixing of chains (low parameter autocorrelation; mean = 0.013). Posterior parameter distributions were contained within the bounds of the prior distributions for all parameters, except for migration from the southern to the northern ancestral population (Fig. S5, Supporting information). At least 11 000 genealogies were recorded for each of the eight replicate runs.

IMa2 (Fig. 3A; Table S4, Supporting information) placed divergence between northern and southern populations in the late Pliocene or early Pleistocene [high point $t1 = 2\,380\,269$; 95% highest posterior density (HPD) 1 941 225–3 002 718 years ago], and the split between southern inland and southern coastal populations in the late Pleistocene ($t0 = 64\,435$; 21 812–118 244 years ago). Compared to the ancestral effective population size ($Ne_{ANC} = 85\,688$; 34 700–136 676), sizes of southern ($Ne_S = 488\,098$; 398 317–667 801) and northern ($Ne_{N1} = 424\,677$; 305 779–771 158) populations grew after $t1$, but declined dramatically after $t0$ in all three descendant populations: southern coastal ($Ne_{SC} = 23\,369$; 12 039–47 447), southern inland ($Ne_{SI} = 29\,035$; 14 871–53 112) and northern ($Ne_{N2} = 242\,901$; 138 092–626 727) (Fig. 3A; Table S4, Supporting information). Even though gene flow was likely underestimated due to omitting admixed individuals from the IMa2 analysis, our results showed nonzero nuclear gene flow between all ancestral and all current genetic populations (Fig. 3A; Table S4, Supporting information). For the $t1$-to-$t0$ time period, forward-in-time gene flow from south to north ($m2 = 5.8$; 4.2–9.4) was higher than that from north to south ($m1 = 0.4$; 0–1.5). For $t0$-to-present, gene flow from southern to northern populations ($m4 = 5.3$; 1–7.8, $m8 = 0.7$; 0.4–0.9) was higher than that from northern to two southern ones ($m3 = 1.6$; 0.7–2.4, $m7 = 4.5$; 1–6.8), and gene flow from coast to inland ($m6 = 3.8$; 2.5–5.4) was higher than that from inland to coast ($m5 = 1.02$; 0.2–1.5). These nuclear geneflow estimates suggest that neutral gene migration was primarily in the south-to-north direction.

Mitochondrial lineage divergence

Convergence for the combined BEAST run of the 10 protein-coding mitochondrial gene data set was confirmed with trend plots and high effective sample sizes (>2000) for all parameters. The mitochondrial tree reflects the known deep mitochondrial split between mito-A and mito-B, and comparison of this tree to the nDNA structure also reflects the known strong mitonuclear discordance (Fig. 4). Mitolineages mito-A and mito-B were estimated to have diverged in the late Pliocene or early Pleistocene (2 000 000; 1 700 000–2 400 000 years ago; Fig. 4; Table S4, Supporting information). These dates overlap with the 95% HPD of the time of population divergence between northern and southern populations and thus consistent with the prediction that mitochondrial and nuclear divergence coincided temporally. The time to the most recent common ancestor (TMRCA) for mito-A was placed in the mid Pleistocene (276 000—HPD: 213 000–319 000 years ago) and TMRCA for mito-B in the late Pleistocene (90 000—HDP: 56 000–96 000 years ago). These times are recent relative to the divergence time between mitolineages (Figs 3B and 4), presumably because the inland and coastal mitochondrial selective sweeps occurred at these times (Thomson *et al*. 2000; Rambaut *et al*. 2008).

Discussion

We explored whether evolution of mitonuclear discordance in the EYR could be explained by a model of two independent events of mitochondrial introgression leading to perpendicular axes of nuclear and mitochondrial genetic differentiation (Fig. 1C). Coalescent analyses provided evidence of temporally concordant nDNA and mtDNA divergence. This strongly supports our

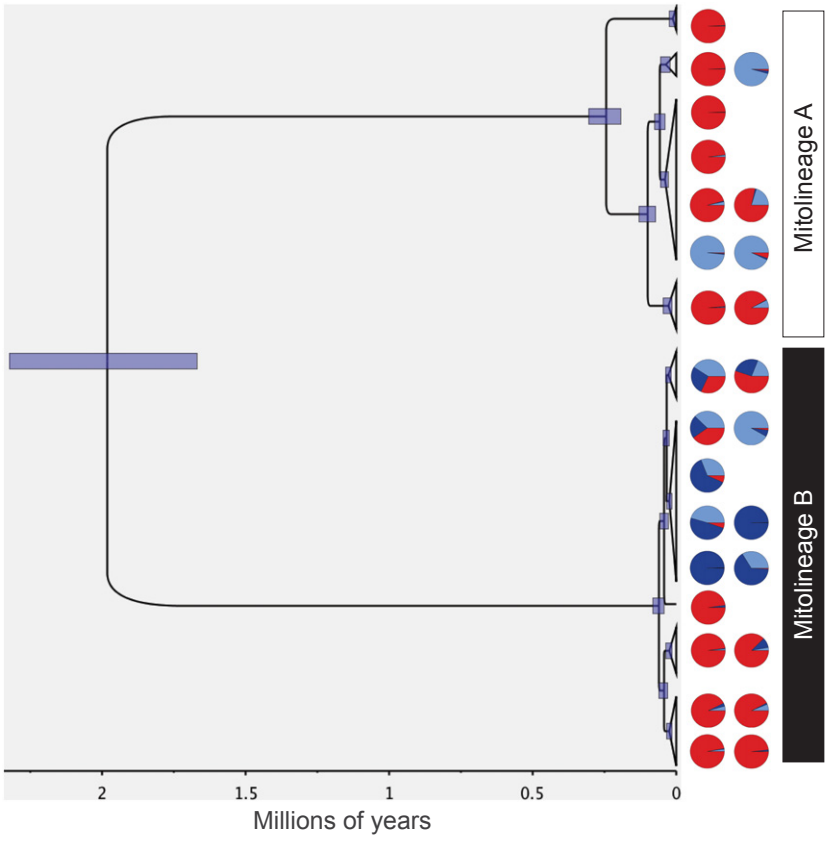

Fig. 4 Phylogenetic tree reconstructed by BEAST from 10 mitochondrial genes. The 95% HDP of the time estimates are shown with blue bars in the tree nodes. The two mitolineages are shown with white (mito-A) and black (mito-B) rectangles as in Fig. 1a. The northernmost sample of mito-A mitolineage displays late Pleistocene intralineage divergence. Samples for which nuclear loci were also sequenced are shown with individual pie charts reflecting their population assignment membership as in Fig. 1b: northern population (red), southern coastal population (dark blue) and southern inland population (light blue). All major nodes are fully supported (PP = 1.0). For more details including node support values, expanded terminal tips and individual labels see Fig. S6.

hypothesis that EYR mitonuclear discordance was caused by population divergence followed by two independent events of mitochondrial introgression. Mitochondrial lineage divergence and introgression generated a deep inland-coastal mitochondrial split within each of the two divergent nuclear genetic backgrounds (north and south; Fig. 1C). One plausible driver of this major shift is adaptive mitochondrial introgression during a period of transition from relatively warm, stable climates with high summer precipitation, to more variable and winter-dominated rainfall climates, and aridification of inland Australia (below) (Hocknull *et al.* 2007; Byrne *et al.* 2008, 2011; Sniderman *et al.* 2009). This process could have had implications for mitonuclear co-introgression because divergent inland-coastal mitochondrial types would need to maintain mitonuclear interactions suitable for metabolic functioning under local environmental variation (Morales *et al.* 2016b). Overall, our data suggest that a first axis of differentiation was formed during north–south divergence-with-gene-flow (reflected in plumage colour subspecies and major nDNA structure, Morales *et al.* 2016a and this study) and was supplemented by a second perpendicular axis of differentiation after two events of mitochondrial introgression generating inland-coast mitochondrial divergence-with-gene-flow (consistent with two deeply divergent mitolineages).

Eastern Yellow Robin evolutionary history

The geographic pattern of nDNA, colour variation and mtDNA in EYR indicate that the concordant early Pleistocene divergence of mtDNA and nDNA occurred in the north–south direction. This is reflected in present-day distributions of nDNA and plumage colour being structured north–south (Fig. 1B; Morales *et al.* 2016a). Mitolineage mito-A is the only population currently occurring in the northern part of the species' range, and it shows evidence of late Pleistocene intralineage vicariance between the northernmost part of its range and the rest of the mitolineage (Figs 1A and 4). Large-scale Pleistocene climatic shifts are likely drivers of the initial north–south divergence (Byrne *et al.* 2008, 2011). Two vicariant/environmental barriers located near the zone of intergradation between northern and southern populations could have facilitated north–south EYR divergence (Fig. 1B). The Hunter Valley Barrier is a dry lowland river valley with low vegetation density that started to form with the opening of the Sydney Basin

during the early Permian (~299 Ma) and continued to be shaped until more recent times with sea levels changes during the Pleistocene (Boyd & Roy 1995; Percival *et al.* 2012). The Southern Transition Zone is a region between lowlands and highlands of the central Great Dividing Range that experience intermittent periods of glaciation and preglaciation during the Pleistocene (Barrows *et al.* 2002). These two barriers have been implicated in subspeciation in several bird species and other closed-forest taxa including invertebrates, lizards, frogs, mammals and plants (Ford 1987; Schodde & Mason 1999; Schodde 2006; Bryant & Krosch 2016).

Given the clear pattern of north–south historical divergence, we can explain the current mitonuclear discordance in EYR by invoking two instances of long-range introgression of mitolineages that became fixed with little associated nuclear introgression (Fig. 1C). Estimating with certainty where in space the initial north–south divergence occurred is not possible, because any number of demographic events could have overwritten the genetic signal of population structure. However, two lines of evidence support the contention that divergence occurred somewhere in the vicinity of the current north–south contact zone (Fig. 1B). First, hundreds of genomewide genetic markers support divergence at this region (Fig. S4, Supporting information). Second, previous geographic cline analyses showed that genetic and plumage colour clines have their centre estimates (i.e. maximum rate of frequency change) at the contact zone, suggesting that colour evolution is a by-product of neutral genetic divergence that occurred near this geographic region (Morales *et al.* 2016a). Accepting the population scenario just described, we can infer the direction and time of introgression by the geographic positions of mitolineages and the estimated time of mitochondrial sweeps (Figs 1C and 3B). The data can be explained if northern mito-A introgressed southwards along the inland side of the Great Dividing Range in the mid Pleistocene, while southern mito-B introgressed northwards along the coast in the late Pleistocene. Thereafter, in the southern population only, nDNA is inferred to have sorted into coastal and inland populations, concordant with the mitochondrial split (Figs 1 and 3A).

Mitochondrial DNA introgression was likely adaptive

Showing conclusive evidence of fitness effects of mtDNA introgression in wild populations is challenging. First steps towards demonstrating adaptive mtDNA introgression, however, come from rejecting scenarios of neutral introgression, and strong genetic evidence of non-neutral evolution (Ballard & Melvin 2010; Boratyński *et al.* 2014; e.g. Doiron *et al.* 2002; Llopart *et al.* 2014). Our current data do not provide for a definitive test for adaptive mitochondrial introgression, but several major patterns in the data are not congruent with selectively neutral scenarios.

Consistently with theoretical expectations, empirical data for birds with female-biased dispersal overwhelmingly show very little mitochondrial flux between hybridizing lineages in a range of contact scenarios (Currat *et al.* 2008; Petit & Excoffier 2009; Rheindt & Edwards 2011; Toews & Brelsford 2012). The migration parameter estimates here and the data in Morales *et al.* (2016a) indicate that gene flow occurred during north–south divergence of EYR. However, we cannot clearly distinguish among alternative models of divergence: secondary contact, primary intergradation and spatial invasion. Thus, interpreting mtDNA vs. nDNA introgression in terms of different population divergence scenarios is challenging (Petit & Excoffier 2009). Despite this limitation, our data are not consistent with neutral introgression under female-biased dispersal. We argue this is because EYR underwent complete mitochondrial replacement with little associated nuclear gene flow over large proportions of the species' range. Further, this divergence occurred in two opposing directions and was correlated with contrasting climates.

Our data on EYR do not agree with nonadaptive explanations for high mitochondrial introgression based on unequal or small effective population sizes and mutation load (Toews & Brelsford 2012; Sloan *et al.* 2016). This is because our coalescent estimates show that ancestral populations had equally large population sizes. We cannot reject outright another class of explanation for high mtDNA flow relating to higher female dispersal (Petit *et al.* 2004) and propensity to mate with available males (Roca *et al.* 2005) as a possible driver of neutral mitochondrial introgression in the north–south direction. However, EYR is among the more sedentary of birds, typically dispersing less than a few kilometres (Debus & Ford 2012; Harrisson *et al.* 2012; Amos *et al.* 2014). Also, the sexes in EYR are very similar in size and appearance and live in territorial pairs, indicating that the mating system is likely to be approximately monogamous and not particularly disposed to exceptionally female-biased gene flow (Higgins & Peter 2002). On balance, we consider that female-biased dispersal alone is implausible as an explanation of inferred mitochondrial introgression in EYR over hundreds of kilometres.

In summary, EYR mitochondrial introgression cannot be explained exclusively by selectively neutral explanations: (i) mitochondrial introgression events in EYR resulted in two cases of near-fixation through large geographic expanses of contrasting environments, in opposite latitudinal directions, accompanied with little signal of nDNA introgression, and (ii) such patterns are

anticipated by evidence of adaptive mitochondrial evolution (selective sweeps, and amino acids in genes plausibly connected the climate adaptation showing signals of positive selection) in this system (Morales *et al.* 2015; Fig. 1; Pavlova *et al.* 2013).

A model of adaptive mitochondrial introgression can explain the demographic, ecological and evolutionary features of EYR introgression history. We propose that first, large ancestral northern and southern population sizes could have promoted the accumulation of adaptive mitochondrial variation in each lineage (Fig. 3A; Kimura *et al.* 1963; Ohta 2002; Camus *et al.* 2015). Later, adaptive alleles could have fully replaced alternative mitochondrial alleles in response to large-scale climatic change, generating the observed mitochondrial selective sweeps in each mitolineage (Byrne *et al.* 2008, 2011; Rieseberg 2009; Rheindt & Edwards 2011). This model of adaptive mitochondrial introgression holds regardless of the assumed spatial model of divergence, and instead depends on large effective population sizes and strong environmental contrasts between inland and coastal regions. Mitochondrial adaptive evolution could have been essential to meet metabolic requirements under differential environmental conditions, leading to increased rates of heat production in colder environments and decreased heat/increased rates of energy production in warmer environments and/or during caloric restriction in drier environments (Wallace 2005; Das 2006). Testing metabolic consequences of introgression requires data on fitness responses to environmental variation and hybridization (e.g. Pereira *et al.* 2014; Boratyński *et al.* 2016).

Perpendicular axes of differentiation in the Eastern Yellow Robin

The most striking and unexpected pattern in Eastern Yellow Robin is that of perpendicular axes of differentiation in which nuclear variation is structured north–south and mitochondrial variation east–west (Fig. 1). Mitonuclear interactions are obvious candidates to be both causes and consequences of the observed population genetic patterns. The strong fitness consequences of mitochondrial DNA variation (Wolff *et al.* 2016) are likely to be amplified through mitonuclear co-evolution of essential metabolic and physiological functions (Bar-Yaacov *et al.* 2012; Deremiens *et al.* 2015; Boratyński *et al.* 2016). On the other hand, disrupted mitonuclear interactions can form strong, long-lasting barriers to gene flow and promote speciation (Dowling *et al.* 2008; Gershoni *et al.* 2009; Burton *et al.* 2013; Hill 2015, 2016). In EYR, one possible explanation for the dramatic reduction of effective population sizes in all three populations at ($t0$) after the onset of mitochondrial introgression is strong selection against hybrids bearing incompatible mitonuclear combinations (Fig. 3). Evidence from laboratory crosses across a wide range of animal systems shows that mitonuclear incompatibility fitness effects in hybrids include metabolic malfunctioning, low fertility and increased mortality (reviewed in Burton *et al.* 2013; Levin *et al.* 2014).

The common observation of mitonuclear incompatibilities raises the question of how mitochondria in EYR were able to introgress swiftly into divergent genomic backgrounds. A likely explanation is that mitonuclear interactions resulting from introgression were maintained through mitonuclear co-introgression (Beck *et al.* 2015). Morales *et al.* (2016b) offers genomic data to support this idea: genomewide differentiation between coastal and inland populations is concentrated in a ~15.6 Mb region of the genome enriched for nuclear-encoded genes with mitochondrial function that likely co-introgressed with mitogenomes to maintain locally adapted mitonuclear interactions. Behavioural, metabolic and physiological experiments are required to explore the mechanisms by which coastal and inland populations maintain their mitonuclear divergence (e.g. Hill & Johnson 2013; Boratyński *et al.* 2016; McFarlane *et al.* 2016). One set of predictions arise from the hypothesis that birds from mitonuclear lineages should be able to recognize each other and mate assortatively (i.e. the mitonuclear sexual selection hypothesis; Hill & Johnson 2013).

Despite the large amount of data amassed for EYR, it remains unclear whether either or both of the perpendicular axes of differentiation will lead to speciation. Our data show the importance of understanding phenotypic and mitonuclear diversity patterns before arriving at taxonomic conclusions. Speciation is a complex process that operates along a continuum, and under the biological species concept, the trajectory towards full speciation in EYR seems to be impeded for now (Seehausen *et al.* 2014; Shaw & Mullen 2014). The real challenge for taxonomy then may be that of upon which criteria one can meaningfully, or indeed whether one should, diagnose any intraspecific populations, for example on plumage and nDNA, or on mtDNA. On the other hand, biological and conservation implications of EYR intraspecific variation are clearer: evidence for natural selection operating in different directions and evidence for restricted gene flow on historical timescales indicate that EYR populations are genetically and ecologically nonexchangeable (Crandall *et al.* 2000).

Drivers of differentiation in Eastern Australia

Detailed reconstruction of Quaternary climates in Australia is limited by a paucity of suitable fossil sites, a relatively narrow range of modern climate space for

calibration, and large regional variability (Hocknull *et al.* 2007; Sniderman *et al.* 2009; Porch 2010; Sniderman 2011; Saltré *et al.* 2016). However, there is consensus on key paleoclimatic phenomena that could have driven perpendicular differentiation in EYR. The most important of these are: (i) a major transition in the early Pleistocene from relatively warm, stable climates with high summer precipitation, to later more variable ones characterized by winter-dominated rainfall and, (ii) major differences between northern and southern Australia in the severity and timing of increased summer aridity, and (iii) more severe aridity inland than on the coast (Hocknull *et al.* 2007; Byrne *et al.* 2008, 2011; Sniderman *et al.* 2009).

Multiple lines of evidence indicate that warm and moist early Pleistocene climates in Australia persisted until transition to modern winter-dominated rainfall (Sniderman *et al.* 2009). These conditions are likely to have applied broadly across southeastern Australia, and would have been in place during our proposed phase of north–south divergence of EYR. The adaptive introgression that we propose would have occurred during a transition from the mild early Pleistocene climate to more variable climates with winter-dominated rainfall and summer aridity. This period of climate change involved considerable temporal and spatial complexity, such as oscillation between wetter and drier vegetation types and multiple periods of rapid fall in humidity and temperature (Hocknull *et al.* 2007; Sniderman *et al.* 2009; Sniderman 2011; Saltré *et al.* 2016). However, it is clear that this shift occurred later in northern Australia than in the south: a northeastern tropical rainforest fauna 500-280 KYA was replaced by a xeric fauna 205-170 KYA, while the south experienced increasing aridity from as early as 600 KYA (Hocknull *et al.* 2007). In addition, due to the rain-shadow effect of the Great Dividing Range, aridity is more severe inland than on the coast. This pattern also likely developed earlier in southern than northern Australia (Hocknull *et al.* 2007).

We predict that many codistributed species may have been impacted similarly by these widespread paleoclimatic events. If adaptive mitochondrial introgression is common in the Australian avifauna (e.g. Kearns *et al.* 2014; Shipham *et al.* 2015, 2016), then that, coupled with strong shifts in climate-related selective forces, could provide a general explanation for the very high rate (~50%) of mitochondrial paraphyly observed in Australian birds (Joseph & Omland 2009). Accordingly, strong shifts in environmental gradients associated with paleoclimatic cycling could also be a common general mechanism for mitonuclear co-evolution as a driving force in generating genomic conflict and divergence (Hill 2015). Whether similar phenomena have occurred in other taxa, and on other continents with suitable conditions demands further investigation of evolutionary impacts and biodiversity implications of Quaternary climate change.

Acknowledgements

Funding was provided by Australian Research Council Linkage Grant (LP0776322) and the Holsworth Wildlife Research Endowment (2012001942). H.M. was funded by a Monash University with a Graduate Scholarship (MGS), a Faculty of Science Dean's International Postgraduate Research Scholarship, and a Postgraduate Publication Award (PPA) and by the Department of Public Education (SEP) of the Mexican Government. Bioinformatic analyses were undertaken using the Monash Sun Grid high-performance computer facility. We are grateful to Philip Chan for technical support. Field samples were collected for this study under scientific research permits issued by the Victorian Department of Environment and Primary Industries (numbers 10007165, 10005919 and 10005514) and New South Wales Office of Environment and Heritage (SL100886). Individually numbered metal bands were supplied by the Australian Bird & Bat Banding Scheme (ABBBS) under approval 2870-2. We thank Nevil Amos and Richard Major for coordinating the fieldwork and Holly Sitters and Christine Connelly for providing genetic samples from South and East Victoria. We thank Anders Gonçalves da Silva and Biao Wang for inputs regarding data analysis and Kaspar Delhey for valuable discussions that helped to improve the manuscript. We thank Scott Edwards, Mike Webster, Lynna Kvistad and Stephanie Falk for valuable comments on the manuscript. We are grateful to three anonymous reviewers and editor Matthew Miller from Axios Review for helpful comments on the first draft of this manuscript, and Karen Chambers, Frederic Austerlitz and four anonymous reviewers during the *Molecular Ecology* review process. The authors are also grateful to Alan Lemmon for coordinating the hybrid capture sequencing project.

References

Amos JN, Harrisson KA, Radford JQ *et al.* (2014) Species-and sex-specific connectivity effects of habitat fragmentation in a suite of woodland birds. *Ecology*, **95**, 1556–1568.

Antao T, Lopes A, Lopes RJ, Beja-Pereira A, Luikart G (2008) LOSITAN: a workbench to detect molecular adaptation based on a Fst-outlier method. *BMC Bioinformatics*, **9**, 323–327.

Ballard JWO, Melvin RG (2010) Linking the mitochondrial genotype to the organismal phenotype. *Molecular Ecology*, **19**, 1523–1539.

Barrows TT, Stone JO, Fifield LK, Cresswell RG (2002) The timing of the last glacial maximum in Australia. *Quaternary Science Reviews*, **21**, 159–173.

Bar-Yaacov D, Blumberg A, Mishmar D (2012) Mitochondrial-nuclear co-evolution and its effects on OXPHOS activity and regulation. *Biochimica et Biophysica Acta (BBA)-Gene Regulatory Mechanisms*, **1819**, 1107–1111.

Beck EA, Thompson AC, Sharbrough J, Brud E, Llopart A (2015) Gene flow between *Drosophila yakuba* and *Drosophila santomea* in subunit V of cytochrome *c* oxidase: a potential case of cytonuclear cointrogression. *Evolution*, **69**, 1973–1986.

Boratyński Z, Melo-Ferreira J, Alves P *et al.* (2014) Molecular and ecological signs of mitochondrial adaptation: consequences for introgression? *Heredity*, **113**, 277–286.

Boratyński Z, Ketola T, Koskela E, Mappes T (2016) The sex specific genetic variation of energetics in bank voles, consequences of introgression? *Evolutionary Biology*, **43**, 37–47.

Boyd R, Roy DP (1995) *Quatenary Geology of the Hunter Valley: Excursion Guide*. 29th Newcastle Symposium on Advances in the Study of the Sydney. Department of Geology, Newcastle. NSW: The Univesity of Newcastle. http://digsopen.minerals.nsw.gov.au/?rin=R00049952.

Bryant LM, Krosch MN (2016) Lines in the land: a review of evidence for eastern Australia's major biogeographical barriers to closed forest taxa. *Biological Journal of the Linnean Society*, **119**, 238–264.

Burton RS, Pereira RJ, Barreto FS (2013) Cytonuclear genomic interactions and hybrid breakdown. *Annual Review of Ecology, Evolution, and Systematics*, **44**, 281–302.

Byrne M, Yeates D, Joseph L *et al.* (2008) Birth of a biome: insights into the assembly and maintenance of the Australian arid zone biota. *Molecular Ecology*, **17**, 4398–4417.

Byrne M, Steane DA, Joseph L *et al.* (2011) Decline of a biome: evolution, contraction, fragmentation, extinction and invasion of the Australian mesic zone biota. *Journal of Biogeography*, **38**, 1635–1656.

Camacho C, Coulouris G, Avagyan V *et al.* (2009) BLAST+: architecture and applications. *BMC Bioinformatics*, **10**, 1–9.

Camus MF, Wolf JB, Morrow EH, Dowling DK (2015) Single nucleotides in the mtDNA sequence modify mitochondrial molecular function and are associated with sex-specific effects on fertility and aging. *Current Biology*, **25**, 2717–2722.

Crandall KA, Bininda-Emonds OR, Mace GM, Wayne RK (2000) Considering evolutionary processes in conservation biology. *Trends in Ecology & Evolution*, **15**, 290–295.

Currat M, Ruedi M, Petit RJ, Excoffier L (2008) The hidden side of invasions: massive introgression by local genes. *Evolution*, **62**, 1908–1920.

Das J (2006) The role of mitochondrial respiration in physiological and evolutionary adaptation. *BioEssays*, **28**, 890–901.

Debus S, Ford H (2012) Responses of Eastern Yellow Robins *Eopsaltria australis* to translocation into vegetation remnants in a fragmented landscape. *Pacific Conservation Biology*, **18**, 194–202.

DePristo MA, Banks E, Poplin R *et al.* (2011) A framework for variation discovery and genotyping using next-generation DNA sequencing data. *Nature Genetics*, **43**, 491–498.

Deremiens L, Schwartz L, Angers A, Glémet H, Angers B (2015) Interactions between nuclear genes and a foreign mitochondrial genome in the redbelly dace *Chrosomus eos*. *Comparative Biochemistry and Physiology Part B: Biochemistry and Molecular Biology*, **189**, 80–86.

Doiron S, Bernatchez L, Blier PU (2002) A comparative mitogenomic analysis of the potential adaptive value of arctic charr mtDNA introgression in brook charr populations (*Salvelinus fontinalis* Mitchill). *Molecular Biology and Evolution*, **19**, 1902–1909.

Dowling DK, Friberg U, Lindell J (2008) Evolutionary implications of non-neutral mitochondrial genetic variation. *Trends in Ecology and Evolution*, **23**, 546–554.

Drummond AJ, Suchard MA, Xie D, Rambaut A (2012) Bayesian phylogenetics with BEAUti and the BEAST 1.7. *Molecular Biology and Evolution*, **29**, 1969–1973.

Earl DA (2012) STRUCTURE HARVESTER: a website and program for visualizing STRUCTURE output and implementing the Evanno method. *Conservation Genetics Resources*, **4**, 359–361.

Ellegren H (2007) Molecular evolutionary genomics of birds. *Cytogenetic and Genome Research*, **117**, 120–130.

Evanno G, Regnaut S, Goudet J (2005) Detecting the number of clusters of individuals using the software STRUCTURE: a simulation study. *Molecular Ecology*, **14**, 2611–2620.

Ford J (1979) Speciation or subspeciation in the yellow robins? *Emu*, **79**, 103–106.

Ford J (1987) Minor isolates and minor geographical barriers in avian speciation in continental Australia. *Emu*, **87**, 90–102.

Funk DJ, Omland KE (2003) Species-level paraphyly and polyphyly: frequency, causes, and consequences, with insights from animal mitochondrial DNA. *Annual Review of Ecology, Evolution, and Systematics*, **34**, 397–423.

Gershoni M, Templeton AR, Mishmar D (2009) Mitochondrial bioenergetics as a major motive force of speciation. *BioEssays*, **31**, 642–650.

Gonçalves da Silva A (2016) Canberra Workshop: population genetic scripts. *Zenodo*, doi:10.5281/zenodo.48790.

Haldane JB (1922) Sex ratio and unisexual sterility in hybrid animals. *Journal of Genetics*, **12**, 101–109.

Harrison RG (1990) Hybrid zones: windows on evolutionary process. *Oxford Surveys in Evolutionary Biology*, **7**, 69–128.

Harrison RG, Larson EL (2014) Hybridization, introgression, and the nature of species boundaries. *Journal of Heredity*, **105**, 795–809.

Harrison RG, Larson EL (2016) Heterogeneous genome divergence, differential introgression, and the origin and structure of hybrid zones. *Molecular Ecology*, **25**, 2454–2466.

Harrisson KA, Pavlova A, Amos JN *et al.* (2012) Fine-scale effects of habitat loss and fragmentation despite large-scale gene flow for some regionally declining woodland bird species. *Landscape Ecology*, **27**, 813–827.

Hedrick PW (2013) Adaptive introgression in animals: examples and comparison to new mutation and standing variation as sources of adaptive variation. *Molecular Ecology*, **22**, 4606–4618.

Hey J (2010) Isolation with migration models for more than two populations. *Molecular Biology and Evolution*, **27**, 905–920.

Hey J, Nielsen R (2004) Multilocus methods for estimating population sizes, migration rates and divergence time, with applications to the divergence of *Drosophila pseudoobscura* and *D. persimilis*. *Genetics*, **167**, 747–760.

Higgins P, Peter J (2002) *Volume 6: Pardalotes to Shrike-Thrushes. Handbook of Australian, New Zealand and Antarctic Birds*. Oxford University Press, Melbourne.

Hill GE (2015) Mitonuclear ecology. *Molecular Biology and Evolution*, **32**, 1917–1927.

Hill GE (2016) Mitonuclear coevolution as the genesis of speciation and the mitochondrial DNA barcode gap. *Ecology and Evolution*, **22**, 5831–5842.

Hill GE, Johnson JD (2013) The mitonuclear compatibility hypothesis of sexual selection. *Proceedings of the Royal Society of London B: Biological Sciences*, **280**, 20131314.

Hocknull SA, Zhao J-X, Feng Y-X, Webb GE (2007) Responses of quaternary rainforest vertebrates to climate change in Australia. *Earth and Planetary Science Letters*, **264**, 317–331.

Jakobsson M, Rosenberg NA (2007) CLUMPP: a cluster matching and permutation program for dealing with label

switching and multimodality in analysis of population structure. *Bioinformatics*, **23**, 1801–1806.
Jombart T, Ahmed I (2011) adegenet 1.3-1: new tools for the analysis of genome-wide SNP data. *Bioinformatics*, **27**, 3070–3071.
Jombart T, Devillard S, Balloux F (2010) Discriminant analysis of principal components: a new method for the analysis of genetically structured populations. *BMC Genetics*, **11**, 94–109.
Joseph L, Omland KE (2009) Phylogeography: its development and impact in Australo-Papuan ornithology with special reference to paraphyly in Australian birds. *Emu*, **109**, 1–23.
Kearns AM, Joseph L, Toon A, Cook LG (2014) Australia's arid-adapted butcherbirds experienced range expansions during Pleistocene glacial maxima. *Nature Communications*, **5**, 3994, doi: 10.1038/ncomms4994.
Kimura M, Maruyama T, Crow JF (1963) The mutation load in small populations. *Genetics*, **48**, 1303–1312.
Lanfear R, Calcott B, Ho SY, Guindon S (2012) PartitionFinder: combined selection of partitioning schemes and substitution models for phylogenetic analyses. *Molecular Biology and Evolution*, **29**, 1695–1701.
Lee JY, Edwards SV (2008) Divergence across Australia's Carpentarian barrier: statistical phylogeography of the red-backed fairy wren (*Malurus melanocephalus*). *Evolution*, **62**, 3117–3134.
Lemmon AR, Emme SA, Lemmon EM (2012) Anchored hybrid enrichment for massively high-throughput phylogenomics. *Systematic Biology*, **61**, 721–744.
Lerner HR, Meyer M, James HF, Hofreiter M, Fleischer RC (2011) Multilocus resolution of phylogeny and timescale in the extant adaptive radiation of Hawaiian honeycreepers. *Current Biology*, **21**, 1838–1844.
Levin L, Blumberg A, Barshad G, Mishmar D (2014) Mitonuclear co-evolution: the positive and negative sides of functional ancient mutations. *Frontiers in Genetics*, **5**, 448.
Li H, Durbin R (2009) Fast and accurate short read alignment with Burrows-Wheeler transform. *Bioinformatics*, **25**, 1754–1760.
Li R, Zhu H, Ruan J *et al.* (2010) De novo assembly of human genomes with massively parallel short read sequencing. *Genome Research*, **20**, 265–272.
Llopart A, Herrig D, Brud E, Stecklein Z (2014) Sequential adaptive introgression of the mitochondrial genome in *Drosophila yakuba* and *Drosophila santomea*. *Molecular Ecology*, **23**, 1124–1136.
Mallet J (2005) Hybridization as an invasion of the genome. *Trends in Ecology & Evolution*, **20**, 229–237.
McFarlane SE, Sirkiä PM, Ålund M, Qvarnström A (2016) Hybrid dysfunction expressed as elevated metabolic rate in male Ficedula flycatchers. *PLoS ONE*, **11**, e0161547.
Morales HE, Pavlova A, Joseph L, Sunnucks P (2015) Positive and purifying selection in mitochondrial genomes of a bird with mitonuclear discordance. *Molecular Ecology*, **24**, 2820–2837.
Morales HE, Pavlova A, Sunnucks P *et al.* (2016a) Neutral and selective drivers of colour evolution in a widespread Australian passerine. *Journal of Biogeography*, **44**, 522–536.
Morales HE, Pavlova A, Amos N *et al.* (2016b) Mitochondrial-nuclear interactions maintain a deep mitochondrial split in the face of nuclear gene flow. *bioRxiv*, doi:10.1101/095596.
Narum SR (2006) Beyond Bonferroni: less conservative analyses for conservation genetics. *Conservation Genetics*, **7**, 783–787.
Nei M (1973) Analysis of gene diversity in subdivided populations. *Proceedings of the National Academy of Sciences*, **70**, 3321–3323.
Ohta T (2002) Near-neutrality in evolution of genes and gene regulation. *Proceedings of the National Academy of Sciences*, **99**, 16134–16137.
Pavlova A, Amos JN, Joseph L *et al.* (2013) Perched at the mitonuclear crossroads: divergent mitochondrial lineages correlate with environment in the face of ongoing nuclear gene flow in an Australian bird. *Evolution*, **67**, 3412–3428.
Payseur BA (2010) Using differential introgression in hybrid zones to identify genomic regions involved in speciation. *Molecular Ecology Resources*, **10**, 806–820.
Percival I, Meakin N, Sherwin L, Vanderlaan T, Flitcroft P (2012) Permian fossils and palaeoenvironments of the northern Sydney Basin. *New South Wales. Geological Survey of NSW Quarterly Notes*, **138**, 1–23.
Pereira RJ, Barreto FS, Burton RS (2014) Ecological novelty by hybridization: experimental evidence for increased thermal tolerance by transgressive segregation in *Tigriopus californicus*. *Evolution*, **68**, 204–215.
Petit RJ, Excoffier L (2009) Gene flow and species delimitation. *Trends in Ecology and Evolution*, **24**, 386–393.
Petit RJ, Bodénès C, Ducousso A, Roussel G, Kremer A (2004) Hybridization as a mechanism of invasion in oaks. *New Phytologist*, **161**, 151–164.
Porch N (2010) Climate space, bioclimatic envelopes and coexistence methods for the reconstruction of past climates: a method using Australian beetles and significance for Quaternary reconstruction. *Quaternary Science Reviews*, **29**, 633–647.
Pritchard JK, Stephens M, Donnelly P (2000) Inference of population structure using multilocus genotype data. *Genetics*, **155**, 945–959.
Prum RO, Berv JS, Dornburg A *et al.* (2015) A comprehensive phylogeny of birds (Aves) using targeted next-generation DNA sequencing. *Nature*, **526**, 569–573.
Pyron RA, Hsieh FW, Lemmon AR, Lemmon EM, Hendry CR (2016) Integrating phylogenomic and morphological data to assess candidate species-delimitation models in brown and red-bellied snakes (Storeria). *Zoological Journal of the Linnean Society*, **177**, 937–949.
R Development Core Team (2014) *R: A Language and Environment for Statistical Computing*. R Foundation for Statistical Computing, Vienna. ISBN 3-900051-07-0.
Rambaut A, Pybus OG, Nelson MI *et al.* (2008) The genomic and epidemiological dynamics of human influenza A virus. *Nature*, **453**, 615–619.
Rambaut A, Suchard M, Xie D, Drummond A (2014) Tracer v1.6. Available from http://beast.bio.ed.ac.uk/Tracer.
Rheindt FE, Edwards SV (2011) Genetic introgression: an integral but neglected component of speciation in birds. *The Auk*, **128**, 620–632.
Rieseberg LH (2009) Evolution: replacing genes and traits through hybridization. *Current Biology*, **19**, R119–R122.
Roca AL, Georgiadis N, O'Brien SJ (2005) Cytonuclear genomic dissociation in African elephant species. *Nature Genetics*, **37**, 96–100.
Saltré F, Rodríguez-Rey M, Brook BW *et al.* (2016) Climate change not to blame for late quaternary megafauna extinctions in Australia. *Nature Communications*, **29**, 10511, doi: 10.1038/ncomms10511.
Schodde R (2006) Australia's bird fauna today–origins and evolutionary development. In: *Evolution and Biogeography of Australasian Vertebrates* (eds Merrick JR, Archer M, Hickey G, Lee M), pp. 413–458. Auscipub, Oatlands, New South Wales.

Schodde R, Mason I (1999) *Directory of Australian Birds: Passerines: Passerines*. CSIRO Publishing, Melbourne.
Seehausen O, Butlin RK, Keller I *et al.* (2014) Genomics and the origin of species. *Nature Review Genetics*, **15**, 176–192.
Shaw KL, Mullen SP (2014) Speciation continuum. *Journal of Heredity*, **105**, 741–742.
Shipham A, Schmidt DJ, Joseph L, Hughes JM (2015) Phylogenetic analysis of the Australian rosella parrots (Platycercus) reveals discordance among molecules and plumage. *Molecular Phylogenetics and Evolution*, **91**, 150–159.
Shipham A, Schmidt DJ, Joseph L, Hughes JM (2016) A genomic approach reinforces a hypothesis of mitochondrial capture in eastern Australian rosellas. *The Auk*, **134**, 181–192.
Sloan DB, Havird JC, Sharbrough J (2016) The on-again, off-again relationship between mitochondrial genomes and species boundaries. *Molecular Ecology*, doi: 10.1111/mec.13959 [Epub ahead of print].
Sniderman J (2011) Early Pleistocene vegetation change in upland south-eastern Australia. *Journal of Biogeography*, **38**, 1456–1470.
Sniderman J, Porch N, Kershaw AP (2009) Quantitative reconstruction of early Pleistocene climate in southeastern Australia and implications for atmospheric circulation. *Quaternary Science Reviews*, **28**, 3185–3196.
Thomson R, Pritchard JK, Shen P, Oefner PJ, Feldman MW (2000) Recent common ancestry of human Y chromosomes: evidence from DNA sequence data. *Proceedings of the National Academy of Sciences*, **97**, 7360–7365.
Toews DP, Brelsford A (2012) The biogeography of mitochondrial and nuclear discordance in animals. *Molecular Ecology*, **21**, 3907–3930.
Wallace DC (2005) A mitochondrial paradigm of metabolic and degenerative diseases, aging, and cancer: a dawn for evolutionary medicine. *Annual Review of Genetics*, **39**, 359–407.
Warren WC, Clayton DF, Ellegren H *et al.* (2010) The genome of a songbird. *Nature*, **464**, 757–762.
Winter DJ (2012) MMOD: an R library for the calculation of population differentiation statistics. *Molecular Ecology Resources*, **12**, 1158–1160.
Woerner AE, Cox MP, Hammer MF (2007) Recombination-filtered genomic datasets by information maximization. *Bioinformatics*, **23**, 1851–1853.
Wolff JN, Pichaud N, Camus MF *et al.* (2016) Evolutionary implications of mitochondrial genetic variation: mitochondrial genetic effects on OXPHOS respiration and mitochondrial quantity change with age and sex in fruit flies. *Journal of Evolutionary Biology*, **29**, 736–747.

Data accessibility

Data access in https://doi.org/10.6084/m9.figshare.3581004.v2:

Sample Information
Hybrid capture probes design
BLAST output file
Fasta alignment files of nDNA loci
SNP data
Alignment of 10 mtDNA genes in nexus format

H.M., A.P. and P.S. designed the research. L.J. provided museum samples. H.M. produced and analysed the data. All the authors contributed to the concepts and paper writing.

Supporting information

Additional supporting information may be found in the online version of this article.

Table S1 Samples screened for nuclear DNA (nDNA) and mitochondrial ND2 variation.

Table S2 Samples screened for mitochondrial genome.

Table S3 Partitions for the BEAST analysis and substitution models according to PartitionFinder.

Table S4 Parameter estimates for coalescent analyses in BEAST and IMa2.

Fig. S1 Convergence plots for STRUCTURE K = 2.

Fig. S2 Convergence plots for STRUCTURE K = 3.

Fig. S3 Delta likelihood for STRUCTURE analysis with populations K = 1–5.

Fig. S4 G_{ST} differentiation between STRUCTURE K = 3 populations.

Fig. S5 Posterior distributions for IMa2 model.

Fig. S6 Phylogenetic tree reconstructed by BEAST from 10 mitochondrial genes.